Comparative analysis of Nafion-functionalized few-layered *vs.* multilayered Ti₃C₂Tₓ MXene/SnS₂ nanoflowers for ammonia detection with enhanced selectivity

Waqas Saeed, [ID][a] Ye Tian,*[a] Irshad Ahmad Mir, [ID] *[b] Baoji Miao,[b] Amna Manzoor,[c] Surjyakanta Rana[d] and Xing Chen[a]

Ammonia (NH₃) detection at room temperature under varying humidity conditions is crucial for environmental monitoring, industrial safety, and healthcare. However, ammonia detection remains a challenge due to the lack of sensitivity and selectivity of current room temperature based sensors. In this context, Ti₃C₂Tₓ MXene and flower-like SnS₂ composites were investigated for NH₃ sensing. A comparative analysis of multilayered and few-layered nanohybrid composites demonstrated that the few-layered configuration displayed a markedly enhanced response to ammonia. Its larger surface area, higher electrical conductivity, and higher number of active sites contribute to its superior gas diffusion and charge transfer properties. The composite was further functionalized with Nafion (NF) to enhance sensitivity and selectivity under humid conditions. In an optimized NF-functionalized few-layered Ti₃C₂Tₓ/SnS₂ sensor, we achieved a 12.11 response ratio towards 100 ppm NH₃, with a response time of 42 s and a recovery time of 156 s, as well as excellent selectivity towards interfering gases. Reliability tests conducted in humid environments confirmed the excellent operational stability and durability of the proposed sensor. These experimental results demonstrate that the developed few-layered Ti₃C₂Tₓ/SnS₂/NF nanohybrid composite provides a highly durable, sensitive, and selective platform for NH₃ detection in practical applications at room temperature.

Introduction

Our atmosphere contains a large amount of ammonia (NH₃), which is primarily generated by three processes: bacterial nitrogen fixation, salt deposition, and combustion from vehicles and industries. It is a part of many raw materials, such as fertilizers, textiles, chemicals, and paper.[1] However, NH₃ is also a very harmful gas. Exposure to NH₃ can result in headaches, vomiting, eye and lung irritation, and, at extremely high levels, even death. Any leak spreads swiftly over a large area due to its light and volatile nature.[2] The hazards associated with NH₃ exposure have been shown by health standards. A human nose can only detect it at levels above 25 ppm, but the Occupational Safety and Health Administration (OSHA) sets a safety limit of

no more than 50 ppm at workplaces.[3] Exposure to an ammonia concentration of approximately 100 ppm, even for a short duration, is believed to be hazardous to human health. Therefore, to address these serious issues associated with human health, it is of utmost importance to produce a low-cost, highly sensitive, and selective ammonia gas sensor.

Researchers have extensively focused on metal oxide-based NH₃ gas sensors due to their low cost and simple fabrication method.[4,5] These sensors have very limited practical applications due to their low selectivity and high operational temperature, *i.e.* 150–350 °C.[6,7] To overcome these challenges, scientists have developed alternative materials, such as conducting polymers, transition metal dichalcogenides, transition metal carbides and their composites. In recent years, gas sensing research has focused a lot on MXenes. MXenes are two-dimensional (2D) transition metal carbides,[8,9] with a general formula of M$_{n+1}$X$_n$T$_x$ (n = 1, 2, or 3), where M is an early transition metal, X is carbon or nitrogen, and T$_x$ is any surface termination group like –OH, –O, or –F.[10] Researchers considered using multilayered Ti₃C₂Tₓ, a single-transition-metal carbide MXene, in gas sensing applications because of its high conductivity, high functional group structure, and large specific surface area.[1,11,12] In the stacked configuration, the

aSchool of Mechanical and Electrical Engineering, Henan University of Technology, Zhengzhou 450001, China. E-mail: yetian@haut.edu.cn

bHenan International Joint Laboratory of Nano-Photoelectric Magnetic Material, School of Materials Science and Engineering, Henan University of Technology, Zhengzhou 450001, China. E-mail: mirirshad09@gmail.com

cColloidal and Computational Lab, Department of Chemistry, Government College University Faisalabad, Faisalabad 38000, Pakistan

dCentre for Functional and Surface Functionalized Glass, Alexander Dubček University of Trenčín, 911 50 Trenčín, Slovakia

nanosheets maintain good electrical conductivity due to the intrinsically metallic nature of $Ti_3C_2T_x$ and the formation of continuous electron transport pathways. However, the close interlayer stacking restricts gas diffusion, limiting molecular accessibility and reducing the number of exposed active sites. Considering these structural constraints, adopting a very few-layered $Ti_3C_2T_x$ form offers clear advantages. The few layers expose more surfaces and provide a larger space between the layers so that gas molecules can access them easily and charges can move faster. With its open structure, few-layered MXene promotes faster surface reactions, making it a more efficient and responsive material for surface-driven applications.[13] MXenes are prone to oxidation when exposed to air or moisture and also suffer from low sensitivity, which limits their long-term stability. Therefore, they are often combined with other materials to form composites that enhance their structural integrity and environmental resistance.

Several transition metal dichalcogenides (TMDs) like WS_2, MoS_2, $MoSe_2$, and SnS_2 have received attention for ammonia gas detection in recent years because of their unique electronic properties resulting from their low-dimensional structure.[14–17] In this category, two-dimensional transition metal dichalcogenides have been reported to form stable nanohybrids with other layered materials owing to their similar lattice structures and minimal lattice mismatch.[18] Consequently, TMDs are now considered to be promising alternatives to traditional metal oxides used in ammonia gas sensing. Among transition metal dichalcogenides, SnS_2 is characterized as a top-tier material because of its distinctive chemical and physical properties.[19] With a narrow band gap of about 2.2 eV and a high electrical sensitivity to gas molecules, it is highly suitable for sensing ammonia at room temperature.[20] However, factors such as humidity sensitivity and slow response or recovery still limit the standalone performance of SnS_2.[21,22] This limitation arises from the low electrical conductivity and moisture-induced surface adsorption effects of SnS_2, which slow down gas interaction and recovery processes.[14,23] Combining SnS_2 with conductive MXenes has become very popular in this area. MXenes have a lot of active sites, high carrier mobility, and a strong ability to adsorb gas. This makes MXene-based composites attractive for room-temperature ammonia detection because they can transfer charge faster and are more sensitive.[24]

MXene-based composites often encounter challenges in humid environments, where water molecules can strongly interact with the sensing surface. Such humidity effects can influence ammonia adsorption–desorption dynamics and, consequently, affect real-time NH_3 detection performance under ambient conditions. In order to mitigate this issue, various strategies have been employed to regulate the impact of humidity, including plasma treatment, the application of hydrophobic coatings, or the alteration of interfaces among materials.[25] A hydrophobic surface functionalization can make composites more stable, but it can also make them more resistant and slightly less sensitive.[26] Nafion (NF), as a functional reagent, can be a good material for controlling moisture without compromising the ability of the composite to sense ammonia gas because it has a unique balance of hydrophobic fluorocarbon chains and hydrophilic sulfonic acid groups.[27,28] A thin layer of Nafion protects the material from moisture and provides ammonia with abundant adsorption sites, which makes sensors more stable and sensitive for real-time and IoT use.

In the present work, a comparative sensing efficiency analysis of multilayered and few-layered MXene-based nanohybrid composites was conducted for NH_3 sensing. The experimental results revealed that the few-layered MXene-based composite produced a higher response to NH_3. The higher sensing response was due to the greater number of active sites, larger surface area, and higher conductivity of the few-layered MXene. The composite based on the few-layered $Ti_3C_2T_x$ in combination with the flower-like SnS_2 forms effective diffusion channels and improves gas exchange and charge movement. In order to improve selectivity and stable performance under humid conditions, the composite was functionalized with NF. The sulfonic acids in NF react with the oxide and hydroxyl groups on SnS_2 and MXene to form acid–base interactions with NH_3, and the sequential presence of a fluorocarbon backbone on NF prevents interference with moisture. Owing to these effects, the few-layered $Ti_3C_2T_x/SnS_2/NF$ is a highly favorable nanohybrid composite for the real-world applications of stable, selective, and highly sensitive NH_3 detection at room temperature.

Materials and methods

Materials

All the chemicals utilized in this research were of the highest quality and did not need further purification. We obtained titanium (about 300 mesh, 99.99%) and carbon (about 5000 mesh, 99.95%) powders from Shanghai Macklin Co., Ltd. Aluminum (about 500 mesh, 99.95%), hydrofluoric acid (≥40%, AR), and tetramethylammonium hydroxide (TMAOH) were sourced from Shanghai Aladdin Co., Ltd. We acquired $SnCl_4 \cdot 5H_2O$ from Sigma Aldrich and obtained thiourea (99%) from Aojin Chemical. Finally, citric acid anhydrous (99%) and Nafion (5 wt%) were obtained from Shanghai Macklin Co., Ltd.

Preparation of MAX

Elemental powders of Ti, Al, and C in a molar ratio of 3.0 : 1.1 : 1.9 were used for synthesizing the MAX phases. The mixed powders were subjected to planetary ball milling using yttria-stabilized zirconia balls at a 5 : 1 ball-to-powder ratio, rotating at 300 rpm for 16 hours to ensure uniform mixing. The resulting homogeneous mixture was then cold-pressed under 20 MPa into compact discs and placed into alumina crucibles for sintering. In a tube furnace with flowing argon gas, the samples were sintered at a rate of 5 °C per minute until the temperature reached 1500 °C, followed by a hold of 3 hours. Once cooled to room temperature, the sintered material was obtained and processed into fine powder by grinding and sieving through a 325-mesh sieve to produce uniform MAX phase powder.

Preparation of MXene

To start the etching process, 2 g of the MAX phase powder was slowly added to 40 mL of 40% hydrofluoric acid (HF) and

magnetically stirred at 40 °C for 24 hours. After etching, the suspension was diluted with deionized water and transferred to a 50-mL centrifuge tube. It was centrifuged for 5 minutes in order to separate the supernatant. This step was repeated 5–6 times until the pH of the supernatant exceeded 6. We placed the remaining solid in a vacuum oven at 60 °C for overnight drying to obtain the multilayered MXene powder. In the delamination process, 0.5 g of the multilayered MXene powder was mixed with 10 mL of a 10 wt% TMAOH solution and stirred at room temperature for 4 hours. After 4 hours, the solution was centrifuged at 8000 rpm for 5 min, and the resulting solid particles were washed several times using deionized water until the pH was <8. Following this, the resulting powder was ultrasonicated for 1 hour under argon to help facilitate exfoliation. The resulting dark suspension was centrifuged again and subsequently freeze-dried to obtain few-layered MXene sheets.

Preparation of flower-shaped SnS$_2$

The fabrication of a flower-like SnS$_2$ nanostructure was carried out *via* a simple solvothermal method. A total of 225.63 mg of SnCl$_4$·5H$_2$O, 228.36 mg of thiourea, and 210.14 mg of citric acid (CA) were added gradually to ethylene glycol under magnetic stirring and stirred for 60 min to obtain a uniform mixture. The as-prepared mixture solution was transferred to a 100-mL Teflon-lined stainless-steel autoclave and heated to 190 °C for 18 hours. Following the reaction, the Teflon-lined autoclave was allowed to cool to room temperature. The product was centrifuged at 6000 rpm and washed five consecutive times with an aqueous solution of deionized water and ethanol to remove unreacted precursors/impurities. Finally, the product was dried in the oven at 60 °C overnight to obtain the flower-like SnS$_2$ powder.

Preparation of Nafion-functionalized multi/few-layered Ti$_3$C$_2$T$_x$/SnS$_2$ nanohybrid composite

The MXene/SnS$_2$ composite was prepared separately after the synthesis of SnS$_2$ to avoid MXene oxidation, since the high temperature ($\sim$190 °C) used during SnS$_2$ formation could damage its surface. The adopted process for fabrication is illustrated in Fig. 1. For every composite, we placed MXene and
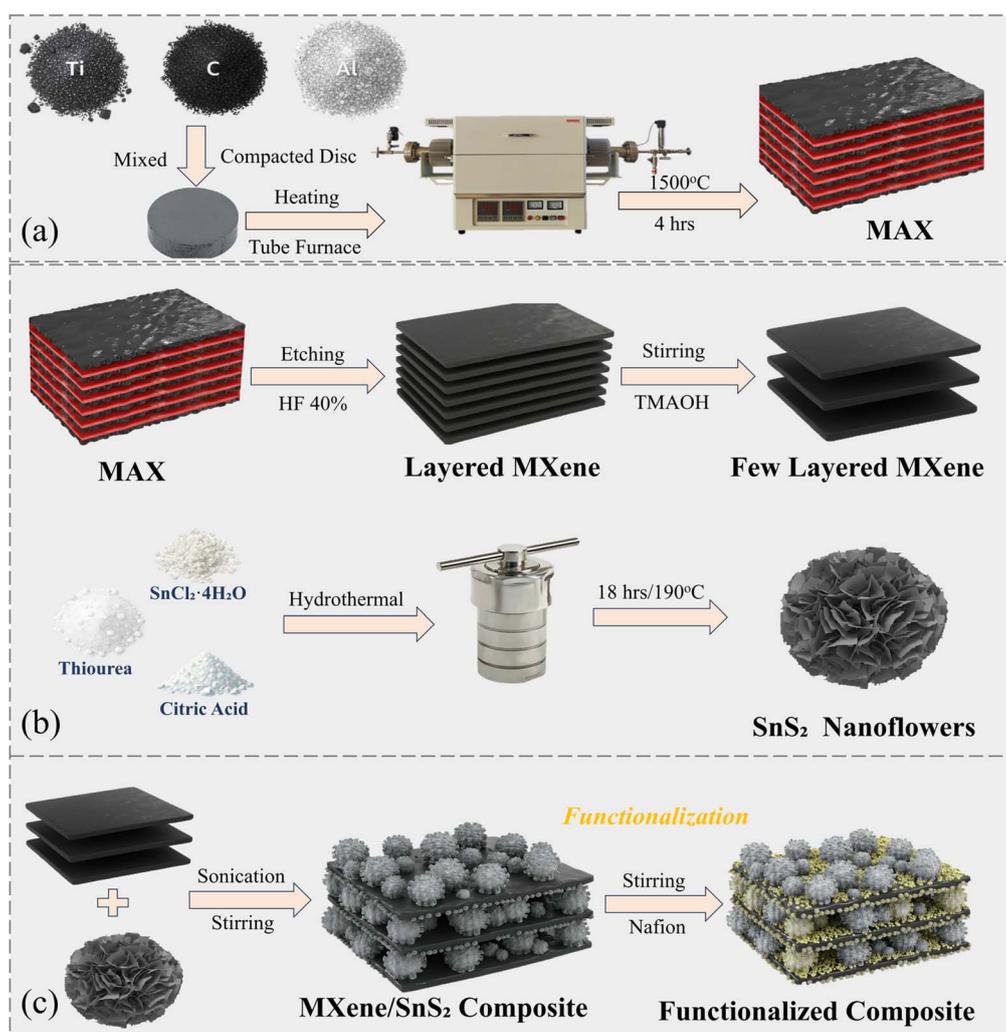

Fig. 1 Schematic of the process adopted to prepare the (a) MAX, (b) few-layered Ti$_3$C$_2$T$_x$ MXene and SnS$_2$ nanoflower, and (c) few-layered Ti$_3$C$_2$T$_x$/SnS$_2$ nanoflower composite.

flower-like SnS_2 in 20 mL of deionized (DI) water separately and used ultrasonication for 15 minutes to make sure that they were evenly mixed. The sonicated SnS_2 suspension was then slowly mixed with the predetermined amount of MXene (10, 20, and 30 wt%).[29] For the few-layered MXene composites, lower concentrations of MXene (8, 10, and 12 wt%) were used because the delaminated layers provide a larger surface area, allowing effective interaction even at reduced loadings.[30,31] The mixture was then ultrasonicated for 3 hours at room temperature to facilitate the even mixing of the MXene/SnS_2 mixtures. The mixture was further stirred at room temperature for 1 hour and then centrifuged at 7000 rpm 2–3 times to prevent large aggregates. The collected precipitates were dried overnight at 60 °C to obtain fine composite powder. Three of the composites containing multilayered $Ti_3C_2T_x$ were labeled Comp-10L, Comp-20L, and Comp-30L. The composites with few-layered MXenes were labeled Comp-8, Comp-10, and Comp-12, according to their MXene contents of 8, 10, and 12 wt%, respectively.

To make the composite more selective for ammonia and less affected by moisture, the few-layered MXene/SnS_2 composite was functionalized with NF. In this study, the NF concentration was optimized to form a thin functional layer that balances humidity tolerance with gas accessibility. An optimal NF loading is known to reduce excessive water uptake and suppress the bulk swelling of NF in high-humidity environments while preserving ionic selectivity. Therefore, three different suspensions were prepared, each containing 80 mg of the composite in 80 : 20 v/v ethanol/deionized water, and ultrasonicated for 15 minutes. After sonication, the suspensions were stirred at room temperature for 1 hour. Then, NF solution was added dropwise in amounts of 0.1, 0.2, and 0.3 mL to the different suspensions that were being stirred.[23] Each suspension was stirred for another 1 hour at room temperature. The samples were uniformly mixed, centrifuged, washed with deionized water 2–3 times, and dried at 60 °C for 6 hours. Finally, the NF-functionalized products were labeled Comp-10 NF@0.1, Comp-10 NF@0.2, and Comp-10 NF@0.3, according to their concentrations of NF.

Characterizations

Through X-ray diffraction (XRD, Bruker D8 ADVANCE), we obtained crystallographic parameters. We then analyzed the types of elements in our samples *via* X-ray photoelectron spectroscopy (XPS, Thermo Scientific ESCALAB 250Xi). The composition and morphology of the samples were then analyzed through field-emission transmission electron microscopy (TEM, FEI Tecnai G2 F30) and field-emission scanning electron microscopy (SEM, FEI INSPECT F50). We examined the chemical bonds of the synthesized composite and functional groups using Fourier-transform infrared (FTIR) spectroscopy.

Gas sensing

The gas-sensing performance of the prepared samples was evaluated using a modified Sino-AGG Tech AES-4SD Flexible Device Analysis System. The sensing measurements were conducted using silver interdigitated electrodes on an alumina

ceramic substrate. In order to prepare the film, 100 mg of the sensing material was dissolved in 1 mL of ethanol and ultrasonically dissolved to obtain a uniform suspension. The resulting paste was drop-cast onto the electrode surface and dried under vacuum at 60 °C for 3 hours. The sensing measurements were performed at a constant applied voltage, where the sensors were exposed to various target gases, including NH_3, CO_2, ethanol, acetone, trimethylamine, and formaldehyde. For baseline comparison under typical indoor dry-air conditions, the response was recorded at 25 °C and 35% relative humidity (RH). The sensor response (S_h) was calculated as the ratio of resistance in the target gas (R_g) to that in air (R_a).

$$S_h = \frac{R_a}{R_g}$$

When the gas is absorbed, it produces a response for the gas through a resistance change. The response time of the sensor is the amount of time it takes for 90% of the total resistance to change. When gas is desorbed, the recovery time is the amount of time it takes to return to 90% of the baseline resistance.

Results and discussion

The crystalline behavior of the MAX phase, $Ti_3C_2T_x$ nanosheets, and all composites was examined through XRD. After etching the MAX, the (104) peak around $2\theta \approx 38.43°$ completely disappeared, and the diffraction peaks between 33° and 43° became much weaker than those of Ti_3AlC_2. This change indicates that aluminum was successfully etched away from the MAX phase. Furthermore, the (002) peak of $Ti_3C_2T_x$ shifted to a lower angle, *i.e.* 7.21°, as shown in Fig. 2(a). These shifts suggest a reduction in structural order and an increase in the spacing between layers, both of which are typical signs of multilayered MXene formation.[32] The delamination treatment of multilayered MXene into few-layered sheets made the (002) peak the most intense and dominant feature in the XRD pattern, shifting it further to 6.19°, as shown in the low-angle XRD pattern in Fig. 2(b). The shift to a lower angle corresponds directly with an increase in the interlayer spacing between the MXene sheets. This is an indication of the delamination process, where the gap between the layers expands as the multilayered structure exfoliates.[33] In the low-angle XRD region, the prominent (002) reflection observed at 6.19° suggests that the delamination process effectively expanded the interlayer distance between the MXene sheets, confirming the formation of few-layered MXene structures. This shift provides valuable insight into the structural changes induced by the delamination treatment. The XRD profile clearly confirmed the successful synthesis of the MAX and few-layered MXene after etching and delamination. The XRD pattern of the SnS_2 nanoflowers displayed distinct peaks at 15.3°, 28.03°, 32.02°, 41.8°, and 50.4°, as shown in Fig. 2(c). These diffraction peaks correspond to the (001), (100), (101), (102), and (110) planes of SnS_2.[14,34] When the few-layered $Ti_3C_2T_x$ MXene was integrated with the SnS_2 nanoflowers to form the nanohybrid composite samples (Comp-8, Comp-10, and Comp-12), noticeable
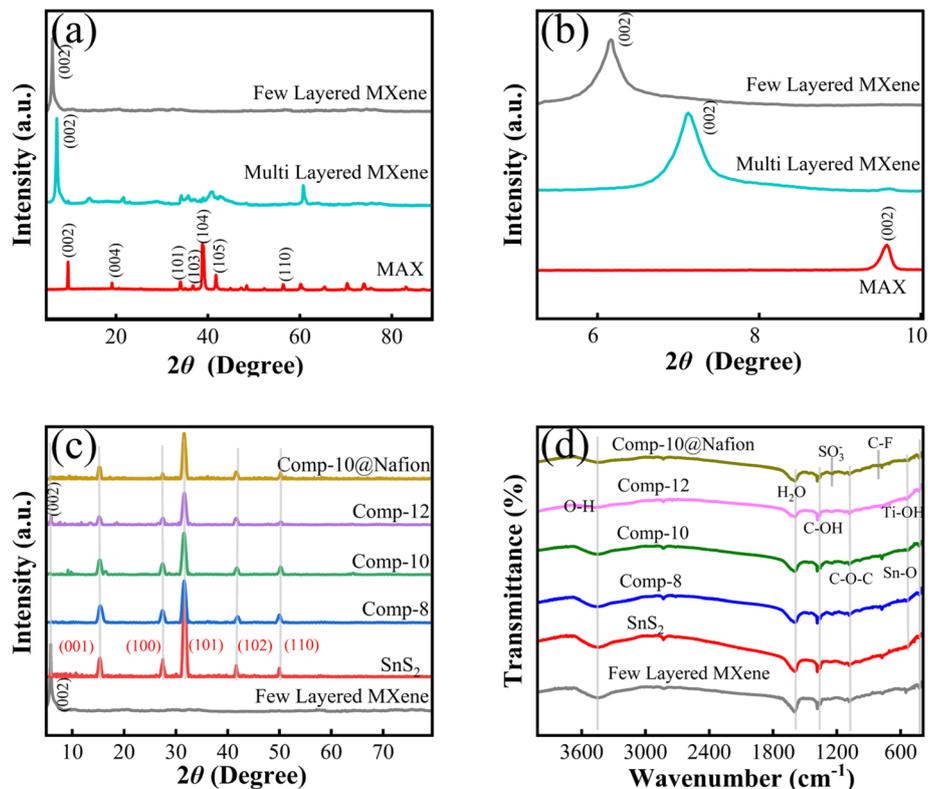
Fig. 2 (a) XRD pattern of MAX and multilayered and few-layered MXene. (b) Low-angle XRD pattern of MAX and MXenes. (c) XRD pattern of few-layered MXene, SnS_2, all composites, and the NF-functionalized composite. (d) FTIR spectra of few-layered MXene, SnS_2, all composites, and the NF-functionalized composite.

variations appeared in their XRD patterns. Among these, only Comp-12 exhibited the characteristic diffraction peaks of MXene at $2\theta = 6.19°$, which correspond to the (002) plane. The lack of MXene peaks in Comp-8 and Comp-10 is probably because of their lower MXene content. Fig. 2(c) shows the XRD pattern of Comp-10 after the addition of 0.2 mL of NF solution. The diffraction peaks are exactly the same as those of the original Comp-10. This means that adding NF does not produce any structural changes in the nanohybrid composite.[27] These results confirm the successful integration of few-layered $Ti_3C_2T_x$ within the SnS_2 framework. They also highlight that the detectability of MXene-related reflections in the XRD patterns is directly dependent on the amount of MXene in the composite.[14]

The Fourier transform infrared (FTIR) spectra of the prepared samples are shown in Fig. 2(d). The absorption bands appearing at 3812 and 1356 cm^{-1} correspond to the vibrations of hydroxyl groups and molecularly adsorbed water (–C–O–H), respectively. As the proportion of MXene increases and the amount of SnS_2 decreases, the intensity of these bands gradually decreases, suggesting a reduced presence of surface hydroxyl species. The feature observed at 1082 cm^{-1} is attributed to the stretching vibration of the C–O–C bond.[35,36] The low-wavenumber absorptions at 422 and 538 cm^{-1} are associated with Ti–OH and Sn–O vibrations, respectively.[37,38] After NF functionalization, two new absorption peaks appear at 1246 cm^{-1} and 790 cm^{-1}, which can be attributed to the

symmetric stretching of the sulfonate group ($–SO_3^-$) and the C–F stretching vibration from the fluorinated NF backbone, respectively.[39] These additional peaks clearly confirm the successful functionalization of NF with the few-layered $Ti_3C_2T_x$/SnS_2 composite surface. Although the overall peak intensities slightly decrease, the main spectral features of SnS_2 and MXene remain visible, indicating that NF forms a thin and uniform coating without altering the core structure of the nanohybrid. In summary, the FTIR analysis demonstrates the consistent evolution of the structure of the MAX phase to MXene and later on to the SnS_2-based composites. The NF-functionalized composite exhibits extra sulfonate and fluorocarbon characteristics, which validate good surface modification without a compromise in the structural integrity or typical bonding arrangement of the composite.

Additionally, scanning electron microscopy (SEM) and high-resolution transmission electron microscopy (HRTEM) were used to study the microstructure and morphology of the gas-sensitive materials. The structure of the MAX phase is confirmed by the SEM images shown in Fig. 3(a), and the MXene produced by HF etching is shown in Fig. 3(b). Fig. 3(c) shows the obtained few-layered MXene after further delamination with the TMAOH solution. The individual sheets are well-separated and uniformly distributed, confirming successful exfoliation. Fig. 3(d) clearly displays the flower-like morphology of SnS_2, providing abundant active sites and a high surface-to-volume
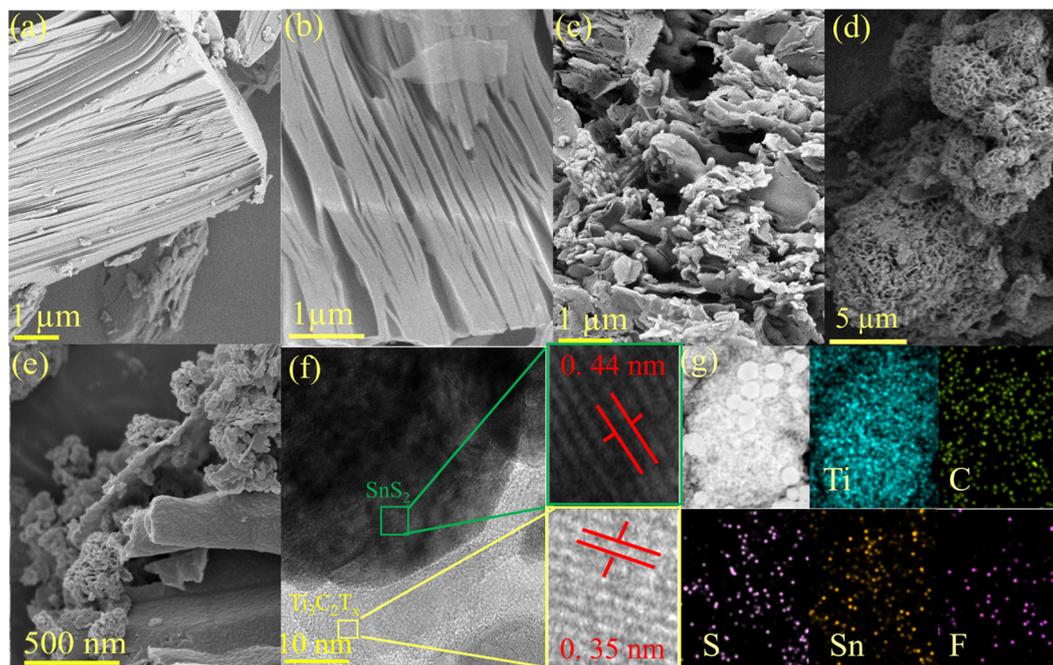
Fig. 3 (a) SEM image of MAX, (b) layered MXene, (c) few-layered MXene, and (d) SnS$_2$ nanoflowers. (e) SEM image of SnS$_2$ nanoflowers attached to the surface of few-layered MXene. (f) High-resolution TEM image of the composite. (g) TEM elemental mapping of Ti, C, Sn, S, F and O.

ratio, both of which are very beneficial for gas adsorption and sensing processes. Fig. 3(e) shows that the SnS$_2$ nanoflowers are attached to the surfaces of the MXene layers. This SEM image is the evidence of the MXene/SnS$_2$ composite system that was already validated by XRD and FTIR. Fig. 3(f) shows the HRTEM image of the MXene sheets with SnS$_2$ nanoflowers attached to their surface. The MXene sheets exhibit a fringe spacing of 0.35 nm, corresponding to the (002) plane, indicating exfoliated few-layered MXene. The SnS$_2$ nanoflowers show a larger fringe spacing of 0.44 nm, attributed to the (001) plane of SnS$_2$, reflecting the interlayer distance of the material. The observed difference in fringe spacing between MXene and SnS$_2$ highlights their distinct structural characteristics. The TEM mapping profile {Fig. 3(g)} confirms the existence of all individual constituent elements in the composite. Additionally, the images demonstrate a uniform distribution of all the elements, which confirms the formation of a composite system.

XPS was employed to obtain further insight into the finer details of the elemental oxidation states of the composites. Fig. 4(a) shows the full elemental spectrum of the composite, making it clear that all the elements are present. Fig. 4(b) shows the Ti 2p spectrum, which can be resolved into three separate peaks. The peak at 454.5 eV is assigned to the Ti–C bonds that are typical of MXene. The peaks at 458.8 eV and 465 eV are assigned to the Ti–O bonds.[40] Fig. 4(c) shows the C 1s spectrum of the Ti$_3$C$_2$T$_x$/SnS$_2$/NF composite, with peaks at 283.8, 284.8, 286.7, and 289 eV. These correspond to Ti–C bonds, neutral carbon (C–C), oxygen-containing groups (C–O), and fluorine-bound carbon (C–F), respectively.[41] The C–C peak reflects unoxidized carbon on the surface, the C–O peak indicates the presence of MXene surface terminations,[12] and the C–F peak

confirms that NF has been successfully functionalized onto the composite. The O 1s spectrum of the Ti$_3$C$_2$T$_x$/SnS$_2$/NF composite {Fig. 4(d)} shows peaks at 530.2, 531.3, 532.7, and 534.0 eV, corresponding to TiO$_2$, C–Ti–O$_x$ surface terminations,[11] –SO$_3^-$ groups from NF,[42] and adsorbed water, respectively. These peaks confirm partial MXene oxidation, the presence of functional groups, and successful NF functionalization. The F 1s spectrum in Fig. 4(e) shows peaks at 684.0, 687.0, and 689.1 eV, corresponding to F–Ti, F–C, and –CF$_2$ bonds, respectively. The F–Ti and F–C signals reflect fluorine bonded to titanium and carbon in the MXene, respectively, while the –CF$_2$ peak arises from fluorocarbon groups, further confirming surface functionalization.[43] The S 2p peaks at 161.8 and 163.2 eV correspond to S 2p$_{3/2}$ and S 2p$_{1/2}$, respectively, and are shown in Fig. 4(f),[44] while the Sn 3d peaks in Fig. 4(g) at 487.0 and 495.4 eV confirm the presence of SnS$_2$.[45] These findings, together with other spectra, confirm successful composite formation and surface functionalization.

Sensing performance evaluation

A two-probe resistive sensor was evaluated at room temperature for the detection of NH$_3$. We measured and recorded the changes in electrical resistance when exposing the sensor to ammonia and air at a constant bias voltage. The sensor was tested at 25 °C and 35% RH as a standard for normal indoor air conditions with dry air. To define the baseline resistance, we measured the response of each constituent material to ammonia, which is presented in Fig. 5. Multilayered MXene had an intrinsically low electrical resistance and exhibited a p-type sensing behavior. The transport characteristics of the materials were identified from their intrinsic electronic properties
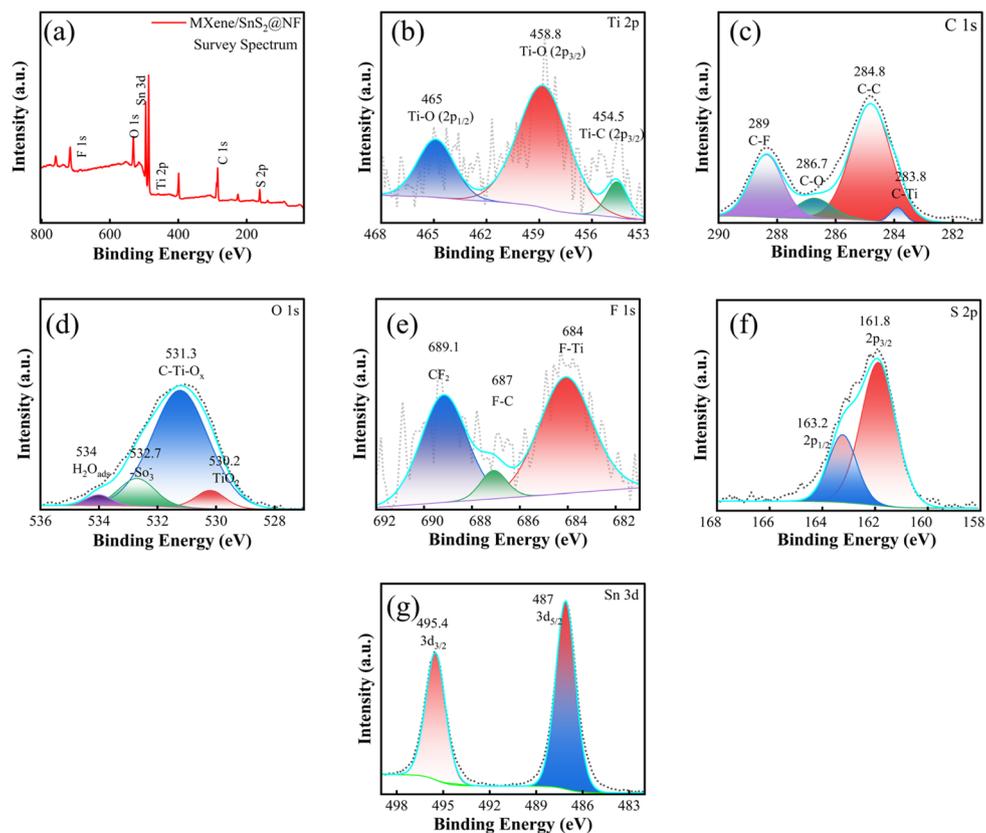
Fig. 4 XPS analysis of the NF-functionalized few-layered $Ti_3C_2T_x$/SnS_2 composite: (a) survey spectrum, (b) Ti 2p spectrum, (c) C 1s spectrum, (d) O 1s spectrum, (e) F 1s spectrum, (f) S 2p spectrum, and (g) Sn 3d spectrum of the functionalized composite.

and gas-response behavior. For example, the MXene showed an increase in resistance when it was exposed to 100-ppm ammonia, as shown in Fig. 5(a), which is a commonly reported behavior for MXene-based sensors.[29,37] $Ti_3C_2T_x$ MXene exhibited

p-type behavior, meaning it conducted electricity through holes (positive charge carriers). This behavior is commonly associated with the presence of surface functional groups, such as –O and –OH, which influence charge transport and lead to hole-
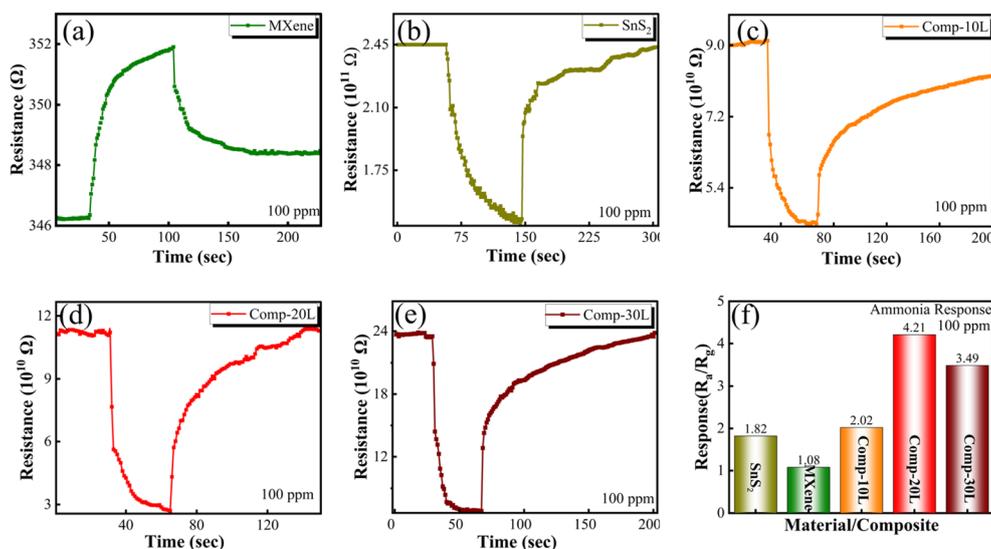
Fig. 5 Base resistance and change in resistance of (a) multilayered MXene, (b) SnS_2, (c) the composite of multilayered MXene/SnS_2 nanoflowers, i.e. Comp-10L, (d) Comp-20L, and (e) Comp-30L upon exposure to 100 ppm ammonia. (f) Response of all materials and composites to 100 ppm ammonia.

dominated conduction characteristics. When exposed to NH_3, the ammonia molecules donated electrons, filling the holes and increasing the resistance, which is typical for p-type materials. When the SnS_2-based sensor was exposed to 100-ppm ammonia, its resistance decreased, as shown in Fig. 5(b). The observed reduction in resistance represents an n-type behavior of SnS_2, where adsorbed NH_3 molecules donate electrons to the material with electrons as the majority charge carriers, increasing its overall charge density and making it more electrically conductive. In order to better understand the interfacial effects and fundamental synergy between the multilayered/few-layered MXene and flower-shaped SnS_2, their composites were examined for ammonia sensing. Initially, the multilayered MXene/SnS_2 composites were synthesized to analyze their gas-sensing performance. Three composites, designated as Comp-10L, Comp-20L, and Comp-30L, were prepared by varying the MXene content. The resistance of these composites decreased upon exposure to 100-ppm ammonia {Fig. 5(c)–(e)}, revealing an n-type sensing behavior, mainly due to the dominant involvement of SnS_2 in the composite. As shown in Fig. 5(f), Comp-20L demonstrated the highest response ratio of 4.21, followed by Comp-30L and Comp-10L.

To compare the sensing performance of multilayered and few-layered MXene/SnS_2 composites and to determine which configuration provides enhanced ammonia detection, few-layered MXene/SnS_2 nanoflower composites were synthesized, and their response to ammonia was investigated. Three samples (named Comp-8, Comp-10, and Comp-12 based on their MXene content) were tested at room temperature with 100-ppm ammonia. Upon exposure, all the composites showed a clear drop in resistance {Fig. 6(a–c)}, confirming their n-type sensing characteristics. As shown in Fig. 6(d), the response intensity varied with the MXene concentration. Comp-10 had the highest response value of 7.02 when exposed to 100-ppm ammonia.

This response value was much higher than those of its counterparts. Therefore, these findings indicate that the Comp-10 ratio is the most effective formulation for maximizing ammonia detection. The results also show that the few-layered MXene combined with SnS_2 nanoflowers has better charge transfer pathways and better surface interactions than the multilayered MXene configuration. The selectivity of Comp-10 was also examined by exposing it to several common environmental gases at 100 ppm {Fig. 6(e)}, including formaldehyde, acetone, trimethylamine, and carbon dioxide. We compared these results with those of the optimized composite of multilayered MXene and individual constituent materials to get a better understanding of the selectivity of all the materials and composites. Although our few-layered MXene-based sensor reacted the strongest with ammonia, it also showed a noticeable cross-sensitivity for other common interfering gases. It is very common for metal sulfide and carbon-based sensors to show a lack of selectivity at room temperature.[46] This cross-sensitivity occurs in these materials because many gases similarly donate electrons to the sensor. Materials like few-layered MXene also promote non-specific gas reactions because of their high surface area.[47] For practical implementation, this is a major challenge, since the sensor must suppress interference from coexisting gases for reliable ammonia detection in complex environments.

An NF solution was used to functionalize the sensor to make it more selective to ammonia. The concentration of NF was optimized to ensure the best performance, as excessive surface functionalization could block active sites, increase overall resistance, and potentially lead to swelling under high-humidity conditions. We tested three concentrations: 0.1 mL, 0.2 mL, and 0.3 mL. The response values for all the functionalized composites are shown in Fig. 7(d). At a 0.1-mL concentration, the response was only 8.03 {Fig. 7(a)}, showing a small increase
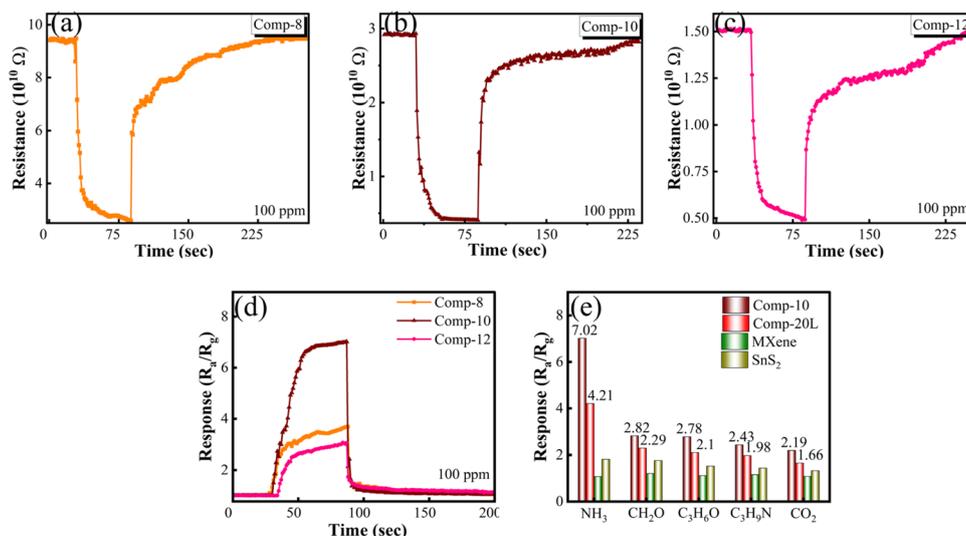

Fig. 6 Base resistance and change in resistance of (a) the composite of few-layered MXene/SnS_2 nanoflowers, *i.e.* Comp-8, (b) Comp-10, and (c) Comp-12 upon exposure to 100 ppm ammonia. (d) Response of all composites to 100 ppm ammonia. (e) Response of few-layered MXene/SnS_2 nanoflowers and multilayered MXene/SnS_2 nanoflowers, MXene and SnS_2 to 100 ppm ammonia and other interfering gases.
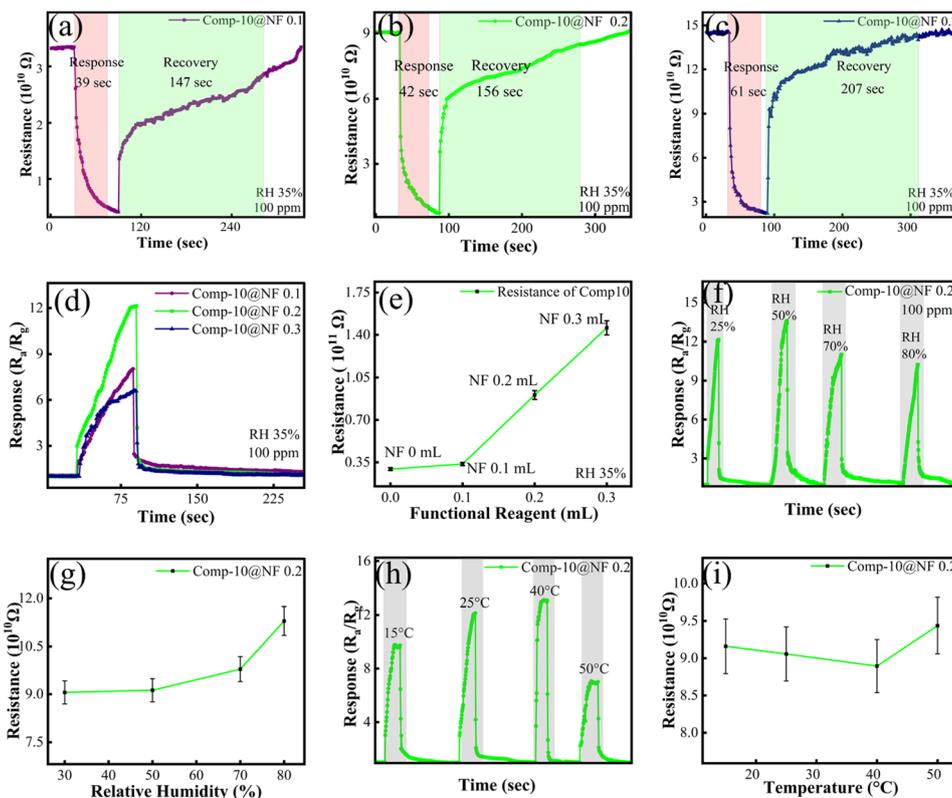
Fig. 7 Base resistance and change in resistance of the optimized composite of few-layered MXene/SnS$_2$ nanoflowers, *i.e.* Comp-10, with varying NF concentrations of (a) 0.1, (b) 0.2, and (c) 0.3 mL, upon exposure to 100 ppm ammonia. (d) Response of all functionalized composites of Comp-10 with NF. (e) Change in base resistance of the optimized composite, *i.e.* Comp-10, with varying NF concentrations. (f) Effect of RH on the response and (g) baseline resistance of the sensor. (h) Effect of temperature on the response and (i) baseline resistance of the sensor.

compared to the unfunctionalized sensor. The results revealed that 0.2 mL was the most effective concentration, yielding the highest response of 12.11 against 100-ppm NH$_3$, with response and recovery times of 42 s and 156 s, respectively {Fig. 7(b)}. The response dropped significantly to 6.58 when the NF concentration was increased to 0.3 mL, as shown in Fig. 7(c). The presence of a moderate concentration of NF (–SO$_3$H groups) enhances the conduction of protons and amplifies the sensitivity of the sensor, as well as the adsorption of ammonia. With a further increase in the concentration of NF, beyond the optimum concentration, it may block active sites and increase resistance, leading to a reduced response. Besides maximizing the response magnitude, the NF concentration also had an effect on the kinetic performance of the sensor. As shown in Fig. 7(c), the higher concentration of 0.3 mL significantly increased the recovery time, while the response time increased marginally. The thicker NF layer traps more ammonia molecules, which makes it take longer to recover because the stronger binding interactions require more energy to desorb the gas.[23] In addition to acting as a gas diffusion barrier that physically hinders gas adsorption and desorption, higher concentrations of NF also have a large impact on the electrical conductivity of the composite material. Fig. 7(e) shows that the baseline resistance of the sensor increased gradually with the NF concentration, reaching its maximum value at 0.3 mL of NF.

This happens because the sulfonic acid (SO$_3$H) groups and fluorocarbons form thicker insulating layers that stop the flow of electrons. In summary, slower ammonia desorption and increased electrical resistance led to a weaker sensing signal and slower response/recovery at higher NF concentrations. Therefore, optimizing the NF concentration is essential for effective composite functionalization.

Subsequent investigations were conducted to systematically evaluate the influence of environmental humidity and operating temperature on the sensing characteristics of the optimized sensor. As the RH increased from 25% to 50%, the sensor response toward NH$_3$ increased, as shown in Fig. 7(f). This can be attributed to the presence of a moderate amount of adsorbed water molecules that enhance surface charge transfer and facilitate the interaction between NH$_3$ and the sensing layer. NF, with its hydrophilic sulfonic groups, can retain limited moisture, promoting proton-assisted conduction and improving gas adsorption at moderate humidity levels. However, further increasing the RH beyond 50% led to a gradual decrease in response, likely due to excessive water adsorption that blocks active sensing sites and competes with NH$_3$ molecules, thereby suppressing effective gas–surface interactions. Meanwhile, the baseline resistance continuously increased with the RH, as shown in Fig. 7(g), and this is associated with increased carrier scattering and reduced charge transport caused by adsorbed

water layers on the sensor surface. The sensor response also showed a strong dependence on the operating temperature. At 15 °C, the response was relatively low because of limited thermal energy, which restricts NH_3 diffusion and surface reaction kinetics, as shown in Fig. 7(h). Increasing the temperature to 40 °C significantly enhanced the response, reaching a maximum value of 13.09, as a higher temperature promotes faster adsorption–desorption dynamics and a more efficient charge transfer. However, when the temperature was further increased to 50 °C, the response decreased to 6.98, which can be attributed to the accelerated desorption of NH_3 molecules and reduced residence time on the active sites. The baseline resistance showed a slight decrease as the temperature increased from 15 °C to 40 °C {Fig. 7(i)}, mainly due to improved charge carrier mobility and thermally activated transport. However, at temperatures above 40 °C, the baseline resistance increased, which can be attributed to the enhanced desorption of surface species and partial suppression of NF-assisted proton conduction, resulting in reduced charge transfer efficiency. Overall, the results confirm that the sensor sustains a consistent ammonia response and manageable baseline variation under changing humidity and temperature conditions, underscoring its robustness for practical sensing applications.

Table 1 summarizes a comparison of the sensing performance of our NF-functionalized $MXene/SnS_2$ sensor with recently reported NH_3 sensors. As shown, our sensor exhibits competitive response values and faster response times compared with most of the reported sensors. In order to investigate the reproducibility and determine the minimum ammonia concentration at which the sensor responds, the NF-optimized sensor was tested over a range of ammonia concentrations from 10 ppm to 100 ppm. Fig. 8(a) shows that the sensor produced a significant response even at low concentrations, with responses of 2.01 and 3.28 at 10 ppm and 25 ppm, respectively. Notably, 10 ppm represents the lowest NH_3 concentration at which a reliable response was recorded under the present experimental conditions. The sensor response exhibited a clear linear trend between 10 and 100 ppm, with no saturation observed. The fitting curves for the sensor's response to NH_3 concentration showed strong linear correlations, with an R^2 value of 0.99. Using these linear fits, we calculated the theoretical limit of detection (LOD) as 8.8 ppm, as shown in

Fig. 8(b). This was determined by dividing the standard deviation (s) of the sensor noise by the slope (s) of the curve three times (LOD = $3\sigma/s$). In order to further verify the sensor's practical reproducibility, we conducted five consecutive air/NH_3 exposure cycles against 10- and 25-ppm NH_3 {Fig. 8(c)}. The sensor exhibited excellent reproducibility over repeated cycles, showing only minor fluctuations in the response, as shown in Fig. 8(d). This stable behavior demonstrates its high efficiency and reliable operational stability under repeated NH_3 exposure. A comparative analysis presented in Fig. 8(e) indicates that the NF-functionalized sensor displayed excellent selectivity towards ammonia. Compared with its unfunctionalized counterpart, the functionalized sensor exhibited significantly higher sensitivity to ammonia than to other interfering gases, including formaldehyde, acetone, trimethylamine, and carbon dioxide. These results confirm that the NF coating imparts strong ammonia detection selectivity. The long-term stability of the sensor was examined under high-humidity conditions to verify its reliability for practical applications, as illustrated in Fig. 8(f). Two optimized sensors were stored under controlled conditions at relative humidity levels of 70% and 80%, while the temperature was maintained at 25 °C for a period of twelve days. The sensing response was measured every 24 hours to evaluate performance stability over time. After 12 days of storage under controlled humidity conditions, the sensor stored at 70% RH responded to 100-ppm ammonia with a response of 11.08, whereas the sensor stored at 80% RH showed a response of 10.23. The sensors showed notable but differential recovery after a 3-day recovery period at 35% RH. The 70% RH sample returned to 11.97 (98.8% of its initial response), while the 80% RH sample recovered to 11.08 (91.5% of its initial response). As a result of a reversible hydration/dehydration cycle, the sensor stored at 70% RH largely regained its activity after 3 days of recovery at 35% RH. In contrast, the sensor stored at 80% RH showed slightly incomplete recovery, primarily due to excessive moisture adsorption that caused temporary surface passivation and slowed ammonia desorption. A minor effect may also come from weak competition between ammonia and the hydrophilic SO_3H sites in NF, which can temporarily trap moisture and slightly delay recovery. However, the stable sensing performance observed over 12 days at varying RH levels indicates that

Table 1 Comparison of the sensing capabilities of the NF-functionalized few-layered $MXene/SnS_2$ sensor and other previously developed $MXene/TMDs$ NH_3 sensors

Material	NH_3 (ppm)	Response time (s)	Recovery time (s)	Response (%)[a] or R_a/R_g or R_g/R_a	Ref.
$Ti_3C_2T_x/SnS_2/NF$	100	42	156	91.7%	This work
$Ti_3C_2T_x/MoS_2$	10	56.8	65	1.47%	48
$Ti_3C_2T_x/SnS_2$	10	161	80	42.9%	29
Nb_2CT_x/SnS_2	100	32	78	89.3%	49
$Ti_3C_2T_x/ReS_2$	50	60	43	7.8%	50
$Ti_3C_2T_x/MoS_2$	100	43.6	40.8	21.1%	51

^{a} Response $= \dfrac{R_a - R_g}{R_a} \times 100 \rightarrow \dfrac{90\,565\,840\,000 - 7\,480\,100\,000}{90\,565\,840\,000} \times 100 = 91.7\%$.
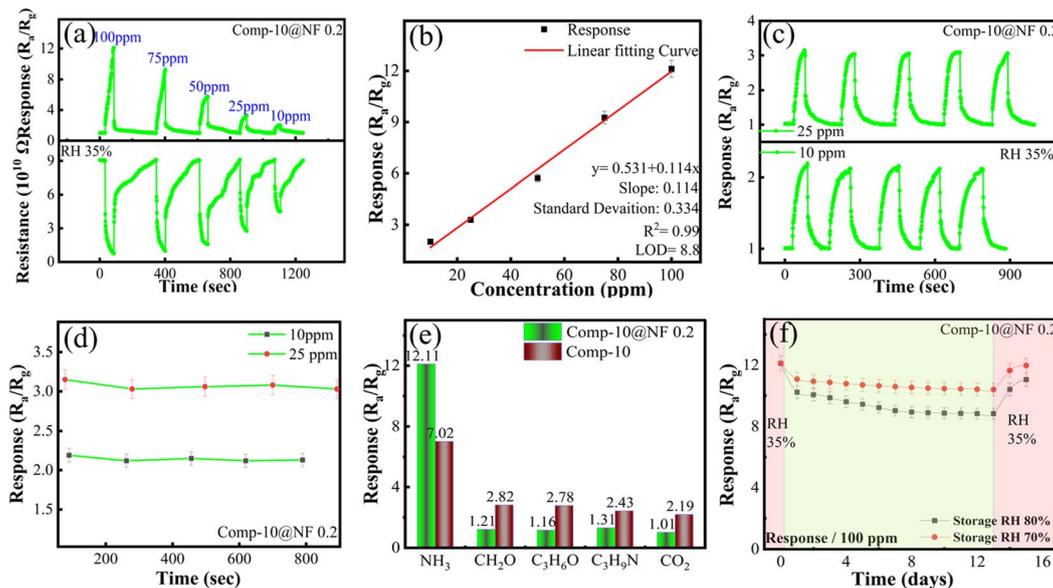
Fig. 8 (a) Reproducibility testing of 0.2 mL Comp-10@NF of 100–10 ppm. (b) Correlation of the response of the sensor with ammonia concentration of 100–10 ppm. (c) Repeatability testing across 25 and 10 ppm concentration. (d) Error bars showing the response variability across each cycle. (e) Response to ammonia and other interfering gases, including comparison with the unfunctionalized Comp-10. (f) Reliability testing at 70% and 80% RH over a period of 12 days.

the optimized NF layer preserves charge transport and gas diffusion.

Sensing mechanism

The sensing performance of the NF-functionalized few-layered MXene/SnS_2 composite arises from the synergy between surface chemistry and electronic modulation. The SO_3H groups in NF create highly polar domains, which react intensively with ammonia by acid/base reactions, and its fluorocarbon backbone inhibits water uptake. In humid environments, NF plays a dual role. In moderate humidity levels, the hydrophilic SO_3H groups facilitate ammonia diffusion by forming transient NH_4^+ species that enhance the interaction with the functional sites. This interaction not only helps in trapping ammonia molecules on the surface but also enhances the gas sensing performance of the composite, as the ammonia molecules are better adsorbed and more likely to react with the sensing surface. Increasing humidity levels can temporarily shift the baseline resistance, but the hydrophobic fluorocarbon chains of NF effectively prevent excessive moisture adsorption, allowing the sensor to maintain a repeatable and stable performance. The band structures of the composite components further enhance the sensing behavior. $Ti_3C_2T_x$ MXene exhibits metallic behavior with its Fermi level in the conduction band,[52] allowing efficient electron transfer. The Fermi level of SnS_2, an n-type semiconductor, is higher than that of MXene, indicating a higher electron concentration.[29] Owing to the work function difference, electrons transfer from the n-type SnS_2 to the higher-work-function $Ti_3C_2T_x$ MXene upon contact, establishing a Schottky junction. This creates an electron depletion region and upward band bending in SnS_2 near the interface. This configuration

greatly enhances the electron exchange and resistance modulation upon gas adsorption, leading to improved sensitivity.

Under ambient air conditions, oxygen molecules adsorb onto n-type SnS_2 and extract electrons from the conduction band, resulting in chemisorbed oxygen species (O_2^-). The corresponding surface reaction is represented by eqn (1) and (2). This process creates an electron depletion layer near the surface and defines the baseline resistance of the sensor, as shown in Fig. 9. When ammonia is present, the strong electron-donating molecules of ammonia react at several active sites in the functionalized composite. NH_3 forms hydrogen bonds with the sulfonic acid's SO_3H at the NF interface and often undergoes partial proton transfer, which forms ion pairs of SO_3^- and NH_4^+, as expressed in eqn (3).[28] This anchoring effect keeps the ammonia molecules localized close to the surface and, hence, enables the efficient transfer of electrons to SnS_2 domains. Furthermore, molecules of NH_3 adsorb onto SnS_2 at the defects and oxygen adsorption sites and give up electrons to the conduction band, as expressed in eqn (4).[29] These donated electrons neutralize the adsorbed oxygen species, thereby reducing their electron-trapping effect and enhancing the n-type conductivity of SnS_2. The excess electrons are subsequently transferred toward the p-type-like MXene domains at the interface, where they recombine with holes, leading to a reduction in the interfacial depletion region. As a result, the interfacial barrier height decreases, causing a significant reduction in sensor resistance. Conclusively, this synergistic interaction among NH_3, NF, SnS_2, and MXene enables the detection of ammonia with a high sensitivity and rapid response. The sensor also has great stability, reproducibility, and selectivity under different humidity conditions, which highlights its feasible application in the real world.
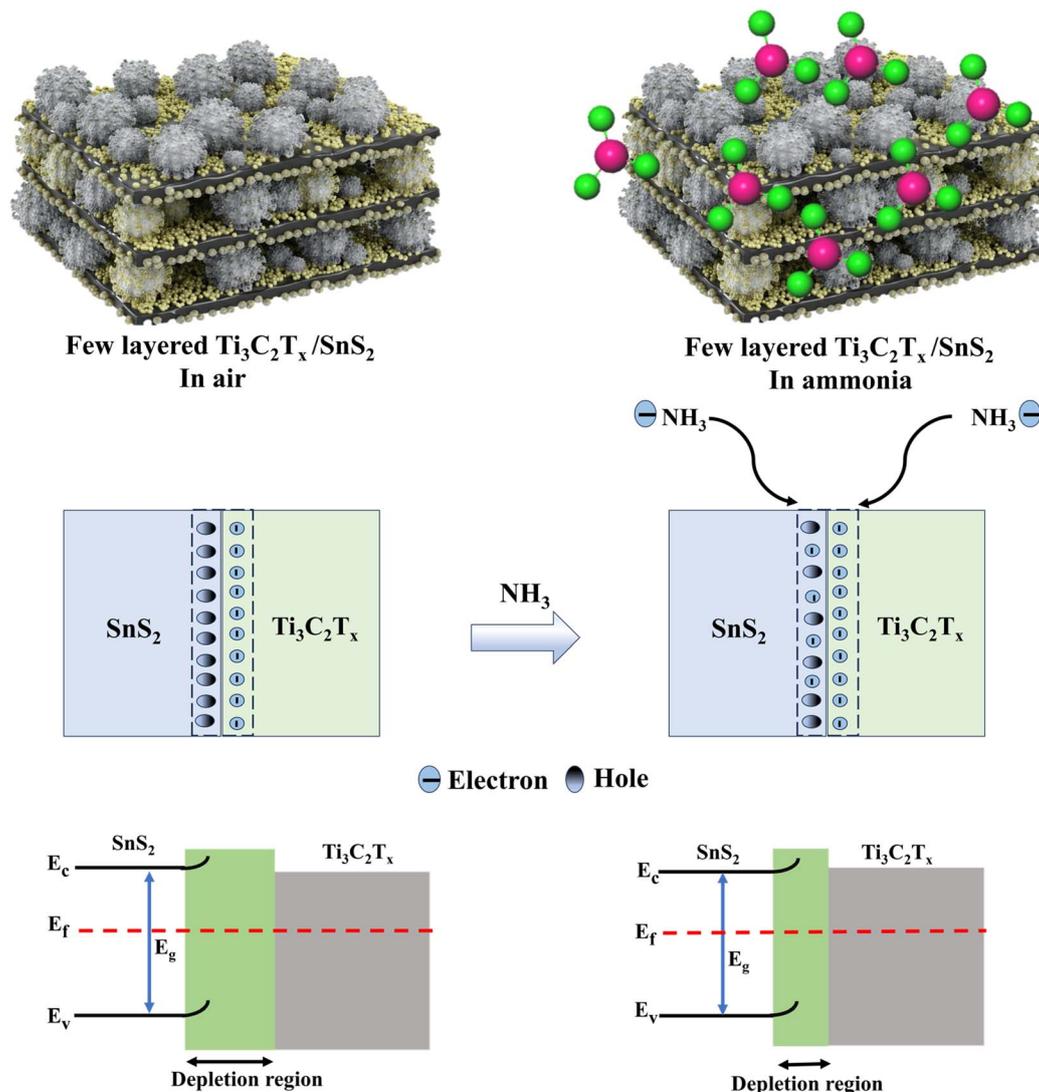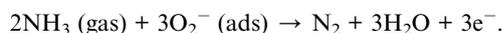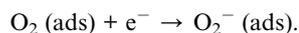
Fig. 9 Gas sensing mechanism of the NF-functionalized $Ti_3C_2T_x/SnS_2$ sensor for ammonia, showing a schematic of the p–n junction and the conductivity pathway changes of the sensor before and after ammonia exposure.

$$O_2 \text{ (gas)} \rightarrow O_2 \text{ (ads)}. \tag{1}$$

$$O_2 \text{ (ads)} + e^- \rightarrow O_2^- \text{ (ads)}. \tag{2}$$

$$SO_3H + NH_3 \rightarrow SO_3^- + NH_4^+. \tag{3}$$

$$2NH_3 \text{ (gas)} + 3O_2^- \text{ (ads)} \rightarrow N_2 + 3H_2O + 3e^-. \tag{4}$$

Compared with the multilayered composites, the few-layered configurations exhibit much better charge transfer and surface interactions, and NF is better at enhancing ammonia adsorption and lowering interference under humid conditions. The sensor also displayed a stable and reproducible performance even under humid conditions, which validated its robustness and effectiveness in long-term real-world applications.

Conclusion

The NF-functionalized few-layered MXene/SnS₂ nanoflower sensor displays excellent room temperature ammonia detection with high sensitivity, fast response (42 s), fast recovery (156 s) and high selectivity. The final optimized composite of the few-layered MXene/SnS₂ nanoflowers coated with 0.2 mL of NF yielded the maximum response of 12.11 to 100-ppm NH₃.

Author contributions

Waqas Saeed: investigation, conceptualization, writing – original draft, methodology, validation, writing – review and editing, formal analysis, data curation and visualization; Ye Tian: fund acquisition and supervision; Irshad Ahmad Mir: resources, visualization, validation and supervision; Baoji Miao, Amna Manzoor, Surjyakanta Rana and Xing Chen: visualization and validation.

Conflicts of interest

The authors declare that they have no known competing financial interests or personal relationships that could have appeared to influence the work reported in this paper.

Data availability

The data supporting the findings of this study are available from the corresponding author upon reasonable request. All relevant experimental details and characterization results are included in the manuscript. No proprietary or confidential data were used.

Acknowledgements

References

1 X. Liang, Z. Chen, H. Wu, L. Guo, C. He, B. Wang, *et al.*, Enhanced NH3-sensing behavior of 2,9,16,23-tetrakis(2,2,3,3-tetrafluoropropoxy) metal(II) phthalocyanine/multi-walled carbon nanotube hybrids: An investigation of the effects of central metals, *Carbon*, 2014, **80**, 268–278, DOI: 10.1016/j.carbon.2014.08.065.

2 X. Liu, N. Chen, B. Han, X. Xiao, G. Chen, I. Djerdj, *et al.*, Nanoparticle cluster gas sensor: Pt activated SnO2 nanoparticles for NH3 detection with ultrahigh sensitivity, *Nanoscale*, 2015, **7**, 14872–14880, DOI: 10.1039/C5NR03585F.

3 R. K. Gangopadhyay and S. Das, Ammonia leakage from refrigeration plant and the management practice, *Process Saf. Prog.*, 2008, **27**, 15–20, DOI: 10.1002/prs.10208.

4 H. Zhu, H. Ji, Z. Yuan, Y. Shen, H. Gao and F. Meng, Highly selective room temperature ammonia gas sensors based on d-band C-SnO2 and response behavior induced by oxidative and reductive role shifts, *J. Mater. Chem. A*, 2023, **11**, 10565–10576, DOI: 10.1039/D3TA01426F.

5 F. Meng, T. Qi, J. Zhang, H. Zhu, Z. Yuan, C. Liu, *et al.*, MoS2-Templated Porous Hollow MoO3 Microspheres for Highly Selective Ammonia Sensing via a Lewis Acid-Base Interaction, *IEEE Trans. Ind. Electron.*, 2022, **69**, 960–970, DOI: 10.1109/TIE.2021.3053902.

6 W. Yan, X. Zeng, G. Wu, W. Jiang, D. Wei, M. Ling, *et al.*, Raspberry-like hollow SnO2-based nanostructures for sensing VOCs and ammonia, *J. Mater. Sci. Mater. Electron.*, 2020, **31**, 14165–14173, DOI: 10.1007/s10854-020-03971-x.

7 X. Xing, Y. Yang, Z. Yan, Y. Hu, T. Zou and Z. Wang, CdO-Ag-ZnO nanocomposites with hierarchically porous structure for effective VOCs gas-sensing properties, *Ceram. Int.*, 2018, **45**(4), 4322–4334, DOI: 10.1016/j.ceramint.2018.11.107.

8 R. Zhang, L. Yang, G. Liu, F. Yin, W. Yuan and S. Guo, Polydopamine functionalized MXene for chemiresistive gas

sensing: partial oxidation and optimized chemical state pinning, *Sens. Actuators, B*, 2023, **386**, 133760, DOI: 10.1016/j.snb.2023.133760.

9 S. Sardana, H. Kaur, B. Arora, D. K. Aswal and A. Mahajan, Self-Powered Monitoring of Ammonia Using an MXene/TiO2/Cellulose Nanofiber Heterojunction-Based Sensor Driven by an Electrospun Triboelectric Nanogenerator, *ACS Sens.*, 2022, **7**, 312–321, DOI: 10.1021/acssensors.1c02388.

10 H. B. Ul, S.-H. Kim, A. Rasool Chaudhry, S. AlFaify, F. K. Butt, S. A. Tahir, *et al.*, Effect of Surface Functional Groups on the Electronic Behavior and Optical Spectra of Mn2N Based MXenes, *ChemPhysChem*, 2024, **25**, e202300605, DOI: 10.1002/cphc.202300605.

11 R. Nag, R. Saha, R. K. Layek and A. Bera, Atomically thin MXene/WSe2 Schottky heterojunction towards enhanced photogenerated charge carrier, *J. Phys. Condens. Matter*, 2024, **36**, 135703, DOI: 10.1088/1361-648X/ad172e.

12 S. J. Kim, H.-J. Koh, C. E. Ren, O. Kwon, K. Maleski, S.-Y. Cho, *et al.*, Metallic Ti3C2Tx MXene Gas Sensors with Ultrahigh Signal-to-Noise Ratio, *ACS Nano*, 2018, **12**, 986–993, DOI: 10.1021/acsnano.7b07460.

13 A. Lipatov, M. Alhabeb, M. R. Lukatskaya, A. Boson, Y. Gogotsi and A. Sinitskii, Effect of Synthesis on Quality, Electronic Properties and Environmental Stability of Individual Monolayer Ti3C2 MXene Flakes, *Adv. Electron. Mater.*, 2016, **2**, 1600255, DOI: 10.1002/aelm.201600255.

14 W. Zhang, W. Wang, Y. Wang, L. Sun, Y. Sun and J. Hu, Au nanoparticles decorated flower-like SnS2/Ti3C2 MXene microcomposite for high performance NO2 sensing at room temperature, *Appl. Surf. Sci.*, 2023, **637**, 157957, DOI: 10.1016/j.apsusc.2023.157957.

15 D. Gu, X. Wang, W. Liu, X. Li, S. Lin, J. Wang, *et al.*, Visible-light activated room temperature NO2 sensing of SnS2 nanosheets based chemiresistive sensors, *Sens. Actuators, B*, 2020, **305**, 127455, DOI: 10.1016/j.snb.2019.127455.

16 D. Xiong, M. Luo, Q. He, X. Huang, S. Cai, S. Li, *et al.*, Nb2CTx/MoSe2 composites for a highly sensitive NH3 gas sensor at room temperature, *Talanta*, 2025, **286**, 127446, DOI: 10.1016/j.talanta.2024.127446.

17 X. Wang, D. Gu, X. Li, S. Lin, S. Zhao, M. Rumyantseva, *et al.*, Reduced graphene oxide hybridized with WS2 nanoflakes based heterojunctions for selective ammonia sensors at room temperature, *Sens. Actuators, B*, 2018, **282**, 290–299, DOI: 10.1016/j.snb.2018.11.080.

18 Y. Liu, N. O. Weiss, X. Duan, H.-C. Cheng, Y. Huang and X. Duan, Van der Waals heterostructures and devices, *Nat. Rev. Mater.*, 2016, **1**, 16042, DOI: 10.1038/natrevmats.2016.42.

19 Q. Zhu, D. Gu, Z. Liu, B. Huang and X. Li, Au-modified 3D SnS2 nano-flowers for low-temperature NO2 sensors, *Sens. Actuators, B*, 2021, **349**, 130775, DOI: 10.1016/j.snb.2021.130775.

20 Y. Huang, W. Jiao, Z. Chu, S. Wang, L. Chen, X. Nie, *et al.*, High Sensitivity, Humidity-Independent, Flexible NO2 and NH3 Gas Sensors Based on SnS2 Hybrid Functional Graphene Ink, *ACS Appl. Mater. Interfaces*, 2020, **12**, 997–1004, DOI: 10.1021/acsami.9b14952.

21 Q. Sun, Y. Li, J. Hao, S. Zheng, T. Zhang, T. Wang, et al., Increased Active Sites and Charge Transfer in the SnS2/TiO2 Heterostructure for Visible-Light-Assisted NO2 Sensing, ACS Appl. Mater. Interfaces, 2021, 13, 54152–54161, DOI: 10.1021/acsami.1c16095.

22 R. Wu, K. Yan, J. Zhao, Z. Cai, S. Jian and L. Qiu, 2D/2D SnS2/SnSe2 van der Waals heterostructure for highly sensitive room-temperature NO2 sensor: Key role of interface contact, Chem. Eng. J., 2023, 466, 143369, DOI: 10.1016/j.cej.2023.143369.

23 K. S. Ranjith, S. Sonwal, A. Mohammadi, G. S. R. Raju, Y. S. Huh and Y.-K. Han, Engineering a surface functionalized Pt@SnS2/Ti3C2Tx MXene sensor with humidity tolerance and high sensitivity at room temperature for NH3 detection, J. Mater. Chem. A, 2025, 13, 2950–2964, DOI: 10.1039/D4TA07108E.

24 W. Quan, J. Shi, H. Luo, C. Fan, W. Lv, X. Chen, et al., Fully Flexible MXene-based Gas Sensor on Paper for Highly Sensitive Room-Temperature Nitrogen Dioxide Detection, ACS Sens., 2023, 8, 103–113, DOI: 10.1021/acssensors.2c01748.

25 G. Xuezheng, S. Yijie, L. Peilin, D. Yanqiao, D. Bingsheng, L. Chengyao, N. Wen, T. Yiling, H. Yuhui, C. Jiangzhao, M. Xiangshui, Y. Xi, et al., Dual Improvement in Sensitivity and Humidity Tolerance of a NO2 Sensor Based on 3-Aminopropyltriethoxysilane Self-Assembled Monolayer-Functionalized SnSe2 for Explosive Photolysis Gas Detection, ACS Appl. Mater. Interfaces, 2023, 15(23), 28358–28369, DOI: 10.1021/acsami.3c02782.

26 W. Y. Chen, S.-N. Lai, C.-C. Yen, X. Jiang, D. Peroulis and L. A. Stanciu, Surface Functionalization of Ti3C2Tx MXene with Highly Reliable Superhydrophobic Protection for Volatile Organic Compounds Sensing, ACS Nano, 2020, 14, 11490–11501, DOI: 10.1021/acsnano.0c03896.

27 M. Lin, Y. Fu, Y. Jin, J. Shi and J. Wei, Investigation of Ammonia-Sensitive Properties of MXene/TiO2/Nafion Composites at Room Temperature, J. Phys., Conf. Ser., 2024, 2920, 012003, DOI: 10.1088/1742-6596/2920/1/012003.

28 D. Sachse, A. Glüsen, K. Wippermann, M. Müller, U. Rau and R. Peters, The Ammonia Adsorption and Desorption Behavior of Nafion, Membranes, 2025, 15, 149, DOI: 10.3390/membranes15050149.

29 T. He, S. Sun, B. Huang and X. Li, MXene/SnS2 Heterojunction for Detecting Sub-ppm NH3 at Room Temperature, ACS Appl. Mater. Interfaces, 2023, 15, 4194–4207, DOI: 10.1021/acsami.2c18097.

30 W. Wang, Y. Yao, J. Xin, X. Zhao, L. Xie and Z. Zhu, Room-temperature highly sensitive triethylamine detection by few-layer Nb2CTxMXene nanosheets, Nanotechnology, 2024, 35, 21, DOI: 10.1088/1361-6528/ad2b4a.

31 G. Feng, S. Wang, S. Wang, P. Wang, C. Wang, Y. Song, et al., Ultra-sensitive trace NO2 detection based on quantum dots-sensitized few-layer MXene: A novel convincing insight into dynamic gas-sensing mechanism, Sens. Actuators, B, 2024, 400, 134852, DOI: 10.1016/j.snb.2023.134852.

32 R. Malik, R. K. Parida, B. N. Parida and N. C. Nayak, EMI shielding behavior of 2D-layered Ti3C2Tx (MXene) incorporated EMA/EOC ternary blend nanocomposites in S-band, J. Mater. Sci. Mater. Electron., 2022, 33, 22599–22613, DOI: 10.1007/s10854-022-09038-3.

33 S. Gong, F. Zhao, Y. Zhang, H. Xu, M. Li, J. Qi, et al., Few-layered Ti3C2Tx MXene synthesized via water-free etching toward high-performance supercapacitors, J. Colloid Interface Sci., 2023, 632, 216–222, DOI: 10.1016/j.jcis.2022.11.063.

34 H. Zhao, B. Zhao, H. Liu and X. Li, Green synthesis of 3D core–shell SnS2/SnS-Cd0.5Zn0.5S multi-heterojunction for efficient photocatalytic H2 evolution, Dalton Trans., 2024, 53, 591–600, DOI: 10.1039/D3DT03533F.

35 E. Lee, A. VahidMohammadi, B. C. Prorok, Y. S. Yoon, M. Beidaghi and D.-J. Kim, Room Temperature Gas Sensing of Two-Dimensional Titanium Carbide (MXene), ACS Appl. Mater. Interfaces, 2017, 9, 37184–37190, DOI: 10.1021/acsami.7b11055.

36 Y.-T. Lin, J.-B. Shi, Y.-C. Chen, C.-J. Chen and P.-F. Wu, Synthesis and Characterization of Tin Disulfide (SnS2) Nanowires, Nanoscale Res. Lett., 2009, 4, 694–698, DOI: 10.1007/s11671-009-9299-5.

37 T. He, W. Liu, T. Lv, M. Ma, Z. Liu, A. Vasiliev, et al., MXene/SnO2 heterojunction based chemical gas sensors, Sens. Actuators, B, 2021, 329, 129275, DOI: 10.1016/j.snb.2020.129275.

38 G. Mangamma, P. K. Ajikumar, R. Nithya, T. N. Sairam, V. K. Mittal, M. Kamruddin, et al., Synthesis and gas phase nitridation of nanocrystalline TiO2, J. Phys. Appl. Phys., 2007, 40, 4597, DOI: 10.1088/0022-3727/40/15/035.

39 C. Chen, G. Levitin, D. W. Hess and T. F. Fuller, XPS investigation of Nafion® membrane degradation, J. Power Sources, 2007, 169, 288–295, DOI: 10.1016/j.jpowsour.2007.03.037.

40 Q. Ta, N. Tri and J.-S. Noh, Improved NO2 gas sensing performance of 2D MoS2/Ti3C2Tx MXene nanocomposite, Appl. Surf. Sci., 2022, 604, 154624, DOI: 10.1016/j.apsusc.2022.154624.

41 L. Li, X. Tian, D. Meng, M. Collins, J. Wang, R. Patterson, et al., Processing, Characterization, and Impact of Nafion Thin Film on Photonic Nanowaveguides for Humidity Sensing, Adv. Photonics Res., 2021, 3(2), 2100181, DOI: 10.1002/adpr.202100181.

42 A. Friedman, W. Shi, Y. Losovyj, A. Siedle and L. Baker, Mapping Microscale Chemical Heterogeneity in Nafion Membranes with X-ray Photoelectron Spectroscopy, J. Electrochem. Soc., 2018, 165, H733–H741, DOI: 10.1149/2.0771811jes.

43 M. Haruta, H. Konaga, T. Doi and M. Inaba, Perfluorinated Ionomer as an Artificial SEI for Silicon Nano-Flake Anode in LiTFSI/Tetraglyme Solvate Ionic Liquid, J. Electrochem. Soc., 2022, 169(2), 020519, DOI: 10.1149/1945-7111/ac4e59.

44 W. Hong, M. Qing, X. He, L. Wang, Y. Pu, Q. Li, et al., Formamide-assisted synthesis of SnS2 nanosheets for high capacity and stable Li-ion battery, J. Solid State Chem., 2023, 330, 124456, DOI: 10.1016/j.jssc.2023.124456.

45 H. Zhang, W. Wang, G. Zhang, X. Wang and J. Cao, 2D/2D SnS2@Ti3C2 MXene heterojunction photocatalyst with

a superior efficiency for tetracycline hydrochloride elimination, *Mater. Lett.*, 2022, **311**, 131550, DOI: 10.1016/j.matlet.2021.131550.

46 P. M. Bulemo, D.-H. Kim, H. Shin, H.-J. Cho, W.-T. Koo, S.-J. Choi, *et al.*, Selectivity in Chemiresistive Gas Sensors: Strategies and Challenges, *Chem. Rev.*, 2025, **125**(8), 4111–4183, DOI: 10.1021/acs.chemrev.4c00592.

47 J. Lemena, R. A. Harris, H. C. Swart, J. J. Terblans and D. E. Motaung, Advances in the engineering of MXenes-based sensors: A transition towards advanced sensing technologies, *Sens. Actuators, B*, 2025, **441**, 137939, DOI: 10.1016/j.snb.2025.137939.

48 S. Sardana and A. Mahajan, Edge-Site-Enriched Ti3C2Tx MXene/MoS2 Nanosheet Heterostructures for Self-Powered Breath and Environmental Monitoring, *ACS Appl. Nano Mater.*, 2023, **6**, 469–481, DOI: 10.1021/acsanm.2c04581.

49 W. Saeed, L. Rasheed, Y. Tian, I. A. Mir, B. Miao, S. Ahmed, *et al.*, Room-Temperature Ammonia Sensing via Nb$_2$CT$_x$/SnS$_2$ Nanocomposite Sensors with Enhanced Selectivity, *Int. J. Miner., Metall. Mater.*, 2025, **33**(4), DOI: 10.1007/s12613-025-3298-0.

50 S. Gasso, J. Carrier, D. Radu and C.-Y. Lai, Novel Gas Sensing Approach: ReS2/Ti3C2Tx Heterostructures for NH3 Detection in Humid Environments, *ACS Sens.*, 2024, **9**, 4788–4802, DOI: 10.1021/acssensors.4c01216.

51 L. Lu, M. Liu, Q. Sui, C. Zhang, Y. Zou, F. Xu, *et al.*, MXene/MoS2 nanosheet/polypyrrole for high-sensitivity detection of ammonia gas at room temperature, *Mater. Today Commun.*, 2023, **35**, 106239, DOI: 10.1016/j.mtcomm.2023.106239.

52 J. K. El-Demellawi, A. E. Mansour, A. M. El-Zohry, M. N. Hedhili, J. Yin, A.-H. M. Emwas, *et al.*, Tuning the Work Function of Ti3C2Tx MXene by Molecular Doping without Changing its Surface Functional Groups, *ACS Mater. Lett.*, 2022, **4**, 2480–2490, DOI: 10.1021/acsmaterialslett.2c00796.